Random Lasing over Gap States from a Quasi-One-Dimensional Amplifying Periodic-on-Average Random Superlattice

Anjani Kumar Tiwari and Sushil Mujumdar*

Nano-optics and Mesoscopic Optics Laboratory, Tata Institute of Fundamental Research, 1, Homi Bhabha Road, Mumbai 400 005, India

(Received 31 January 2013; published 6 December 2013)

We report the experimental implementation and theoretical analysis of a random laser system that constitutes an amplifying periodic-on-average random superlattice (PARS). The stringent conditions on monodispersity required for a periodic-on-average random superlattice system are fulfilled using a linear array of spherical microresonators whose separation and size distribution can be controlled. Statistical studies of the lasing frequency reveal a frequency-controlled behavior. We perform transfer matrix calculations with gain to analyze the origin of the lasing modes, their thresholds, and frequency statistics. The results confirm that the experimentally observed lasing modes arise from states introduced into the stop gap of the underlying periodic system. On virtue of the fact that these high-quality gap states are restricted to a band of frequencies, the consequent random lasing exhibits significant reduction in frequency fluctuations.

DOI: 10.1103/PhysRevLett.111.233903 PACS numbers: 42.55.Zz, 42.25.Dd, 42.25.Hz

Random lasers are a fascinating class of optical amplifying systems [1,2] that exploit structural disorder to realize laserlike emission. The interplay between multiple scattering and optical gain reveals a plethora of exciting phenomena that have generated a great amount of interest [3–16], particularly in the synergy of Anderson localization and optical gain [17–21]. The coupled randomness and gain result in strong frequency and intensity fluctuations [12,22–27]. Recently, literature has focused attention on the frequency behavior of random lasers [10,28–33]. For instance, active spatial control of the excitation in order to strengthen a desired mode has allowed us to control the lasing frequency, effectively "taming" the random laser [29,34]. On the other hand, resonant properties of individual scatterers can be exploited to achieve wavelength control on diffusion and lasing [10,33]. Transport over multiple resonators also induces localization at the wavelengths closest to the resonance [35].

A special kind of disordered system that relies on multiple resonators is the periodic-on-average random system (PARS). It refers to an underlying periodic system that has well-defined bands and band gaps, and is weakly randomized so as to excite localized modes. Here, the localized states can be studied with respect to the band structure of the underlying order. Indeed, one of the earliest seminal works in optical localization dealt with such a system [36]. Recently, massive parallel computations have shown that such systems are most likely to provide localization in three dimensions [37,38]. Significant literature also exists in one-dimensional PARS systems [39–41], including the variation of localization length ξ in the gap [39], enhanced transmission in the gap [40], and statistics of the Lyapunov exponent in PARS systems [41]. On the experimental front, weakly random binary multilayers were created to measure ξ across the band edge [42]. Experimental reports in such systems are relatively few, probably because of twin requirements of (a) monodispersity and (b) a large number of samples for averaging. In the random laser scenario, theoretical works have investigated the statistics of reflection and transmission coefficients in such systems [43,44]. However, to our knowledge, there are no experimental reports of amplifying PARS systems. It is desirable to provide experimental pathways to complement the existing theoretical ideas, in addition to generating new ones. In that regard, we present a practical manifestation of a quasi-one-dimensional amplifying periodic-on-average random superlattice (aPARS). Having recently demonstrated collective lasing from multiple microresonators [45], we analyze the spectral features of these modes from the vantage point of random lasing. Transfer matrices with gain were used to study the frequency behavior of periodic amplifying multilayers and systematically added disorder. The calculations identify the high-quality modes originating from the gap states, whose frequency behavior is in excellent agreement with the experiments. The inherent nature of the gap states leads to frequency-controlled random lasing. Thus, we demonstrate an experimental implementation of an amplifying PARS system. The dynamic nature of our PARS configurations allows us to investigate configurationally averaged quantities, which are most relevant in disordered systems.

We briefly describe the experimental realization of such an aPARS system. The most crucial requirement in an experimental sample is the possibility of controlling the active layer widths to make them monodisperse. This is achieved by employing a technique created for studying ultrahigh-quality microspherical Mie resonators. The microspheres are obtained using a vibrating orifice aerosol

generator that creates microdroplets, using the fracture of an unstable liquid jet [46]. A liquid discharged through a narrow orifice emits as a jet with inherent mechanical instabilities, and spontaneously disintegrates into a stream of polydisperse, irregularly shaped microdroplets. By applying an appropriate periodic perturbation, the unstable jet can be induced to break up into equal-sized droplets. In our setup, the jet is realized by a microcapillary of diameter 10 μm, while the perturbation is created by a piezoelement inside the capillary to which a periodic voltage is applied. We created microdroplets from a Rhodamine 6G-methanol solution, which are emitted serially in a linear configuration. Along the axis of the array, the refractive index profile resembles a multilayer. Under excitation by a Nd:YAG laser ($\lambda = 532$ nm), the array emitted fluorescence in all directions. The transverse (emission perpendicular to the array) and the longitudinal emissions were separately analyzed by a spectrometer ($f = 50$ cm). The longitudinally traveling light experiences the multilayer arrangement, whose widths and separations can be tweaked by modifying the pressure and piezofrequency. The details of microdroplet characterization and the experimental techniques are described in Ref. [45].

Figure 1(a) shows three representative microdroplet arrays, which we identify as polydisperse, aperiodic, and weakly periodic. The top image shows an array of polydisperse microdroplets with random spacings. Shown below the image is the axial refractive index variation, which reflects the randomness in the sizes and the separations in the thus-formed multilayer. We label the mean dimension of the microdroplets along the axis as A and the mean separation as B. The randomness in A (B) is labeled δA (δB), the width of the measured Gaussian distribution in the parameters. In the polydisperse configuration, the parameter set (A, B, δA, δB) was (26.7, 25, 8.3, 24) μm. The middle image shows a monodisperse, aperiodic array with a large randomness in the spacings, where (A, B, δA, δB) = (23.9, 27.8, 0.1, 16) μm. The refractive index profile indicates an aperiodic multilayer with monodisperse active layers. The bottom structure constitutes a weakly periodic multilayer, with (A, B, δA, δB) = (17.1, 6, 0.05, 2) μm. This was the best monodispersity ($\delta A = 0.05$ μm) achieved in the setup. Figure 1(b) shows two shot-to-shot spectra obtained from the longitudinal emission from these configurations. The spectra differ because of the fluctuating configuration. The measurements were made at an excitation energy above threshold, which increased with randomness. In particular, the threshold energies for the three cases were (i) 0.72 μJ, (ii) 0.41 μJ, and (iii) 0.1 μJ, while the excitation energies were (i) 1.7 μJ, (ii) 0.76 μJ, and (iii) 0.32 μJ. The polydisperse sample yields a multimode spectrum with almost overlapping modes, which leads to their broadening. Importantly, the modes appear at random frequencies. The aperiodic sample yields spectra where the modes appear at similar frequencies, and some modal overlap was still seen. The modes from the weakly periodic sample

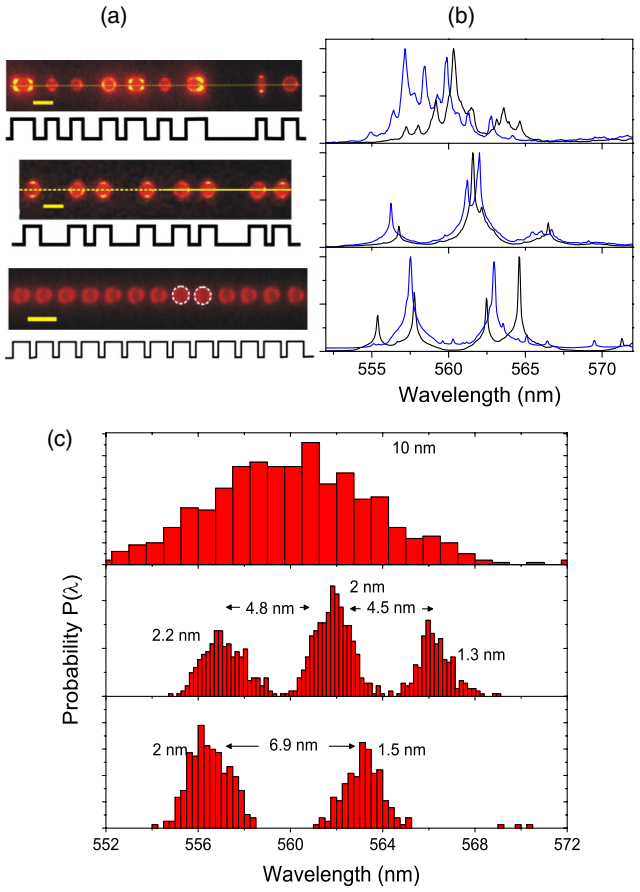

FIG. 1 (color online). (a) Observed aPARS configurations and corresponding axial refractive index profile. Top: Random polydisperse configuration; middle: aperiodic system; bottom: weakly periodic system. Yellow bar: 30 μm. See text for actual dimensions. (b) Spectra from the corresponding systems. (c) Probability distribution of lasing wavelengths in the polydisperse (top), aperiodic (middle), and for a weakly periodic system (bottom).

were fewer in number, and were well separated. They also occurred at comparable frequencies. Occasionally, "doublet" modes (pairs of peaks with equal separations, black spectrum) were seen in the weakly periodic case, but were never observed in the aperiodic configurations. To elucidate the frequency dependence, we plot the frequency distribution of the lasing modes over 200 pump pulses, as shown in Fig. 1(c). The top panel shows the histogram for the polydisperse sample. A wide continuous distribution is seen, which approximately emulates the shape of the gain profile of the dye. No frequency dependence is observed in the emission, reflecting strong frequency fluctuations akin to a conventional coherent random laser. Next, when the size distribution is minimized (middle panel), the continuous distribution breaks into discrete bunches. The immediate restriction in the lasing modes indicates the reduction in frequency fluctuations created by the monodispersity. The histogram bunches range from a width of 1.3 to 2.2 nm, separated by ~4.6 nm. Thus, by minimizing the randomness in size, the system can be made to emit in a

specified wavelength range. Finally, in the weakly periodic manifestation (bottom panel), the separation in the bunches is larger, and the bunch width was limited to 2 nm. The histogram essentially exhibits only two bunches, with evidence of very few modes around $\lambda \sim 571$ nm. This was a consequence of the limited gain profile of the dye, which prevented the formation of lasing modes above $\lambda \sim 568$ nm. We observed that stronger excitation did not compromise the frequency bunching effect; it merely increased the overall number of modes in the spectra and mildly broadened the histogram bunches. Overall, by tweaking the properties of the microdroplet array, the system offered a control of the random lasing frequency.

Conventional dye scatterer–based random lasers rely on the disorder created by nanoscatterers, which are essentially abrupt refractive-index variations in the medium. In this system, the abrupt change of index along the axis of the array realizes multiple reflecting and transmitting interfaces, thereby generating feedback in the longitudinal propagation. Since the individual resonators are quite large compared to the optical wavelengths, the collective mode only encounters an almost planar interface at the axis, and the actual sphericity of the microdroplets does not influence the transport. Essentially, the curved multilayer has such a large radius of curvature at every interface that it can be approximated as a planar multilayer. (This behavior is elucidated using numerical simulations in the Supplemental Material [47].) Therefore, a 1D calculation suffices to analyze the origin of the modes. Accordingly, we model the system as an amplifying multilayer system using 1D transfer matrix calculations [48]. Optical gain is introduced by adding a negative imaginary component to the refractive index of the dielectric (n'-in''), with a Gaussian gain profile centered at $\lambda = 563$ nm and a width of 35 nm. This method is well suited to identify the frequencies of lasing modes and their thresholds, although the suprathreshold behavior cannot be studied because of numerical instabilities [49,50].

Figure 2 shows the transmittance of a passive ($n'' = 0$) PARS system. Here, we discuss systems with arbitrary parameters to gain insight into the effect of randomness. As in the experiments, δA and δB are the widths of the Gaussian distributions of the fluctuations in A and B, respectively. We address a monodisperse system with randomness only in spacings. The red curve depicts the spectrum from a perfectly ordered multilayer ($A, B, \delta A, \delta B = 20, 6, 0, 0$) μm. Two stop bands occur in the region of interest, centered at $\lambda \sim 556$ and 560.7 nm. The modes at the band edge are the highest quality modes, with relatively broader modes in the conduction bands. The introduction of weak randomness in a controlled manner reveals the perturbation of the band-edge states into the stop band. For instance, the blue curve shows a spectrum for a particular random configuration with $\delta B = 0.06$ μm, which corresponds to weak disorder. While the conduction and stop bands still remain defined, the gaps are widened (green arrows) and the erstwhile band-edge modes migrate

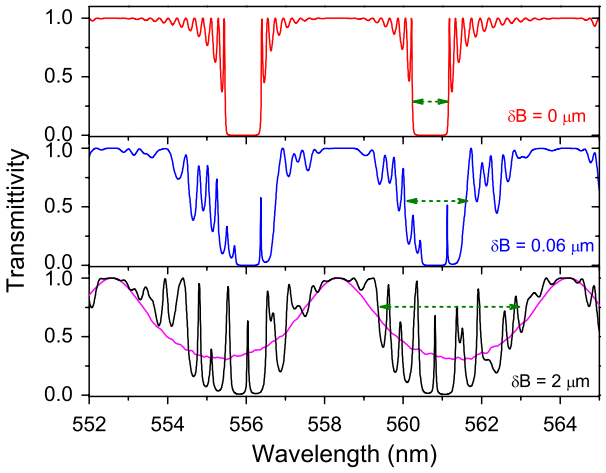

FIG. 2 (color online). Spectra showing the passive transmittance from the ordered system (red curve, top) and from two PARS configurations with separations having weak (blue curve, middle) and strong (black curve, bottom) randomness. Magenta curve: Configurationally averaged transmittance for strong randomness.

into the gap, now known as gap states. The quality factor of these gap states remains high. With increasing disorder ($\delta B = 2$ μm, black curve), several gap states are generated with a distributed Q factor. The configurationally averaged transmittance (magenta curve), the parameter that is usually studied in passive systems, shows equispaced peaks of unit transmittance at separations equal to the free-spectral spacing of an individual layer. These maxima, however, originate from the serial filtering effect from a collection of independent Fabry-Pérot etalons, and are not related to the high-Q modes. Thus, it is of interest to investigate the modes of maximal gain and further interrogate their frequency behavior.

Figure 3 shows the corresponding spectra with optical gain ($n'' = 2.6 \times 10^{-5}$) in all cases, and it was subthreshold in order to avoid numerical instabilities. The highest peaks in the spectra can be identified as the eventual lasing modes. In the periodic system (red curve), the band edges are seen to gain in intensity, as expected of their large quality factor. At each stop gap, the two band edges create a closely spaced (1 nm) pair of lasing peaks, forming a doublet. In the disordered system (blue curve), the modes that lase first are the gap states, reconfirming their high quality factor. The location of these states changes with configuration, while remaining within the gap. Evidently, the "doublet" peaks in the experimental weakly periodic situation [Fig. 1(b), bottom plot] came from some particular instantaneous configuration that had sufficient periodicity to yield band-edge lasing. The inset shows the variation of peak intensity with n'', which identifies the lasing threshold [51]. The gap state had a low lasing threshold ($n'' = 2.77 \times 10^{-5}$), owing to the high quality factor. Under stronger disorder (black spectrum), multiple lasing modes are initiated in the stop gap region, and the lasing threshold is raised to ($n'' = 8.25 \times 10^{-5}$).

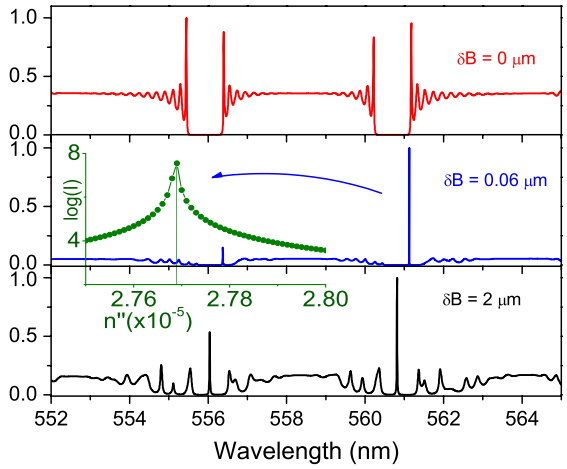

FIG. 3 (color online). Spectral profiles under amplification, for the same configurations as in Fig. 2. The modes in the stop band are seen to lase. Inset: Intensity as a function of n'' for the indicated peak, revealing lasing threshold.

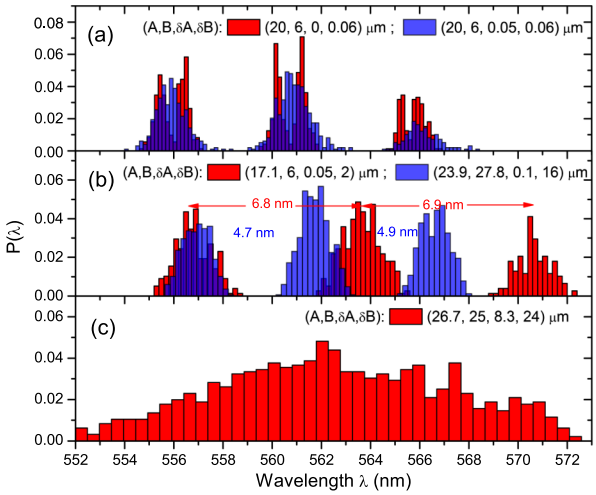

FIG. 4 (color online). (a) Red columns: Lasing wavelength distribution for a weakly disordered system with monodisperse active layers ($\delta A = 0$ μm, $\delta B = 0.06$ μm). Band-edge memory is evident in the double-peaked bunches. Blue columns: Weakly polydisperse system ($\delta A = 0.05$ μm, $\delta B = 0.06$ μm). Band-edge memory is washed out and single-peaked bunches are seen. (b) Simulation of experimental parameters of aperiodic and weakly periodic systems, yielding excellent agreement in the distribution. (c) Continuous, broadband distribution from a strongly disordered system with experimental parameters.

An interesting behavior was revealed in the calculations. The gap mode (blue curve) actually had a lower lasing threshold than the band-edge modes (red curve, $n'' = 5.5 \times 10^{-5}$), because of the higher quality factor of the gap states. Perfect periodicity was inaccessible in the experiments to verify this behavior. However, once the disorder set in, the lasing threshold increased with the disorder, which was in agreement with the experimental observations.

The issue in focus here is the frequency control of the modes, which is quantified in Fig. 4. Figure 4(a) (red histogram) shows the wavelength distribution when the active slabs were perfectly monodisperse $(A, B, \delta A) = (20, 6, 0)$ μm and the separations were weakly randomized with $\delta B = 0.06$ μm. The distribution shows three narrow bunches indicating the restricted wavelengths of the gap modes. Each bunch exhibits a double-peaked profile, showing the memory of the band edges in the gap states. However, the introduction of slight polydispersity (blue plot, $\delta A = 0.05$ μm) washes out the band-edge effect and all bunches show a single peak. This explains the lack of double-peaked bunches in the experimental observation, where an inherent randomness of about 50 nm exists in the microdroplet diameter. At this level of randomness and gain, the central histogram bunch is roughly 1.3 nm wide. Figure 4(b) shows the simulation of the experimental systems (Fig. 1). The blue and the red histograms show the behavior of the weakly periodic system $(A, B, \delta A, \delta B) = (17.1, 6, 0.05, 2)$ μm and the aperiodic system $(23.9, 27.8, 0.1, 16)$ μm, respectively. The experimentally observed frequency control is reproduced as seen from the restricted wavelengths. The mean separations in the bunches are 4.8 and 6.85 nm, respectively, in excellent agreement with experimental separations of 4.65 and 6.9 nm. Because of the extended gain profile in the simulations, we could realize the third bunch in the red histogram. The position of this third bunch coincides with the few modes close to $\lambda \sim 571$ nm seen in the experiments. Despite the large configurational randomness, the frequency bunching effect still occurs because the gain layers remain fairly monodisperse. Thus, δB does not compromise the frequency sensitivity as much as δA. Notably, the bunches are separated by the free-spectral spacing of an individual layer, although the stop gaps of the underlying periodic system are not separated accordingly. This occurs because the disorder widens the averaged stop gaps and makes them equispaced. Finally, when both δA and δB are strongly randomized [Fig. 4(c)], there is no frequency sensitivity in the emission. A continuous distribution of wavelengths is seen, with a width of about 10 nm. Clearly, under such strong disorder, the system can no longer be treated as periodic on average, and behaves like a conventional random laser. These calculations are in excellent agreement with the demonstrated experimental system. Thus, our experimental system behaves as a quasi-one-dimensional aPARS system and offers frequency control of random lasing due to gap states.

In summary, we have realized an amplifying periodic-on-average random system, aPARS. These aPARS systems are promising candidates to study disorder-induced light localization and lasing. This system offers frequency control in coherent random lasers. Further work would involve analyzing the effect of the spherical shape of the droplets, although this will only affect the intensity and interdroplet coupling and not the frequency characteristics. To our knowledge, this is the first demonstration of an aPARS system with conclusive experimental evidence of

frequency control in coherent random lasers. The microdroplet array system promises immediate applications in optofluidic random lasers [15]. Finally, this system offers the opportunity to study the phase transition from a standard (ordered) multimode mode-locked laser to the mode-locked random laser, an issue of great current interest [52–54]. We hope our results trigger more activity in this direction.

We acknowledge Ravitej Uppu and Girish Kulkarni for discussions. S. M. acknowledges support from the DAE, Government of India, and the DST for the Ramanujan Fellowship.

*mujumdar@tifr.res.in; http://www.tifr.res.in/~mujumdar

[1] D. S. Wiersma, Nat. Phys. **4**, 359 (2008).
[2] H. Cao, J. Phys. A **38**, 10 497 (2005).
[3] V. S. Letokhov, Sov. Phys. JETP **26**, 835 (1968).
[4] N. M. Lawandy, R. M. Balachandran, A. S. L. Gomes, and E. Sauvain, Nature (London) **368**, 436 (1994).
[5] M. Noginov, *Solid State Random Lasers*, Springer Series in Optical Sciences Vol. 105 (Springer, New York, 2005).
[6] H. E. Tureci, L. Ge, S. Rotter, and A. D. Stone, Science **320**, 643 (2008).
[7] A. Tulek, R. C. Polson, and Z. V. Vardeny, Nat. Phys. **6**, 303 (2010).
[8] S. K. Turitsyn, S. A. Babin, A. E. El-Taher, P. Harper, D. V. Churkin, S. I. Kablukov, J. D. Ania-Castañón, V. Karalekas, and E. V. Podivilov, Nat. Photonics **4**, 231 (2010).
[9] J. Fallert, R. J. B. Dietz, J. Sartor, D. Schneider, C. Klingshirn, and H. Kalt, Nat. Photonics **3**, 279 (2009).
[10] S. Gottardo, R. Sapienza, P. D. García, A. Blanco, D. S. Wiersma, and C. López, Nat. Photonics **2**, 429 (2008).
[11] S. Mujumdar, M. Ricci, R. Torre, and D. S. Wiersma, Phys. Rev. Lett. **93**, 053903 (2004).
[12] S. Mujumdar, V. Turck, R. Torre, and D. S. Wiersma, Phys. Rev. A **76**, 033807 (2007).
[13] R. Pierrat and R. Carminati, Phys. Rev. A **76**, 023821 (2007).
[14] C. Vanneste, P. Sebbah, and H. Cao, Phys. Rev. Lett. **98**, 143902 (2007).
[15] B. N. S. Bhaktha, N. Bachelard, X. Noblin, and P. Sebbah, Appl. Phys. Lett. **101**, 151101 (2012).
[16] A. K. Tiwari, R. Uppu, and S. Mujumdar, Opt. Lett. **37**, 1053 (2012).
[17] P. Pradhan and N. Kumar, Phys. Rev. B **50**, 9644 (1994).
[18] H. Cao, Y. G. Zhao, S. T. Ho, E. W. Seelig, Q. H. Wang, and R. P. H. Chang, Phys. Rev. Lett. **82**, 2278 (1999).
[19] H. Cao, J. Y. Xu, S.-H. Chang, and S. T. Ho, Phys. Rev. E **61**, 1985 (2000).
[20] X. Jiang and C. M. Soukoulis, Phys. Rev. E **65**, 025601(R) (2002).
[21] V. Milner and A. Z. Genack, Phys. Rev. Lett. **94**, 073901 (2005).
[22] S. Lepri, S. Cavalieri, G.-L. Oppo, and D. S. Wiersma, Phys. Rev. A **75**, 063820 (2007).
[23] X. Wu and H. Cao, Phys. Rev. A **77**, 013832 (2008).
[24] D. Sharma, H. Ramachandran, and N. Kumar, Fluct. Noise Lett. **06**, L95 (2006).
[25] G. Zhu, L. Gu, and M. A. Noginov, Phys. Rev. A **85**, 043801 (2012).
[26] R. Uppu, A. K. Tiwari, and S. Mujumdar, Opt. Lett. **37**, 662 (2012).
[27] R. Uppu and S. Mujumdar, Phys. Rev. A **87**, 013822 (2013).
[28] R. G. S. El-Dardiry and A. Lagendijk, Appl. Phys. Lett. **98**, 161106 (2011).
[29] N. Bachelard, J. Andreasen, S. Gigan, and P. Sebbah, Phys. Rev. Lett. **109**, 033903 (2012).
[30] R. Bardoux, A. Kaneta, M. Funato, K. Okamoto, Y. Kawakami, A. Kikuchi, and K. Kishino, Opt. Express **19**, 9262 (2011).
[31] M. Leonetti, C. Conti, and C. Lopez, Nat. Photonics **5**, 615 (2011).
[32] J. Ripoll, C. M. Soukoulis, and E. N. Economou, J. Opt. Soc. Am. B **21**, 141 (2004).
[33] A. K. Tiwari, R. Uppu, and S. Mujumdar, Photon. Nanostr. Fundam. Appl. **10**, 416 (2012).
[34] N. Bachelard, S. Gigan, X. Noblin, and P. Sebbah, arXiv:1303.1398.
[35] A. A. Chabanov and A. Z. Genack, Phys. Rev. Lett. **87**, 153901 (2001).
[36] S. John, Phys. Rev. Lett. **58**, 2486 (1987).
[37] C. Lopez, Nat. Phys. **4**, 755 (2008).
[38] C. Conti and A. Fratalocchi, Nat. Phys. **4**, 794 (2008).
[39] A. R. McGurn, K. T. Christensen, F. M. Mueller, and A. A. Maradudin, Phys. Rev. B **47**, 13 120 (1993).
[40] V. D. Freilikher, B. A. Liansky, I. V. Yurkevich, A. A. Maradudin, and A. R. McGurn, Phys. Rev. E **51**, 6301 (1995).
[41] L. I. Deych, D. Zaslavsky, and A. A. Lisyansky, Phys. Rev. Lett. **81**, 5390 (1998).
[42] Zhang Daozhong, Hu Wei, Zhang Youlong, Li Zhaolin, Cheng Bingying, and Yang Guozhen, Phys. Rev. B **50**, 9810 (1994).
[43] C.-K. Nam and Z.-Q. Zhang, Phys. Rev. B **66**, 073101 (2002).
[44] X. Jiang and C. M. Soukoulis, Phys. Rev. B **59**, 6159 (1999).
[45] A. K. Tiwari, B. Chandra, R. Uppu, and S. Mujumdar, Opt. Express **20**, 6598 (2012).
[46] H. B. Lin, J. D. Eversole, and A. J. Campillo, Rev. Sci. Instrum. **61**, 1018 (1990).
[47] See Supplemental Material at http://link.aps.org/supplemental/10.1103/PhysRevLett.111.233903 for planar approximation to large curvatures.
[48] S.-H. Chang, H. Cao, and S. T. Ho, IEEE J. Quantum Electron. **39**, 364 (2003).
[49] J. Andreasen *et al.*, Adv. Opt. Photonics **3**, 88 (2011).
[50] X. Jiang, Q. Li, and C. M. Soukoulis, Phys. Rev. B **59**, R9007 (1999).
[51] The decay in the suprathreshold intensity is due to the numerical instability, and has no consequence to the findings reported in this Letter.
[52] R. G. S. El-Dardiry, R. Mooiweer, and A. Lagendijk, New J. Phys. **14**, 113031 (2012).
[53] C. Conti and L. Leuzzi, Phys. Rev. B **83**, 134204 (2011).
[54] L. Leuzzi, C. Conti, V. Folli, L. Angelani, and G. Ruocco, Phys. Rev. Lett. **102**, 083901 (2009).